ORIGINAL
Log & Scan
11/2/00

Prepared for the National Institutes of Health
National Institute of Neurological Disorders and Stroke
Division of Stroke, Trauma and Neurodegenerative Disorders
Neural Prosthesis Program
Bethesda, MD 20892

Microstimulation of the Lumbosacral Spinal Cord: Mapping

NIH-NINDS-NO1-NS-8-2300

Quarterly Progress Report #8

Period Covered: 1 July, 2000 - 30 September, 2000

Principal Investigator: Warren M. Grill, Ph.D.

Co-Investigators: Kenneth J. Gustafson, Ph.D.
Musa A. Haxiu, M.D., Ph.D.
Michel A. Lemay, Ph.D.

Department of Biomedical Engineering
Case Western Reserve University
Cleveland, OH 44106-4912

ABSTRACT

The objectives of this research are to determine the anatomical locations of spinal neurons involved in control of the genitourinary and hindlimb motor systems, and to determine the physiological responses evoked in the genitourinary and hindlimb motor systems by intraspinal microstimulation. During this quarter we made progress toward both of these objectives. We continued a series of experiments using intraspinal injections of retrograde tracers to identify last-order interneurons that project to either the preganglionic innervation of the bladder or the pudendal motoneurons innervating the external urethral sphincter. Secondly, we continued our experiments measuring the hindlimb motor responses evoked by intraspinal microstimulation. In these experiments we began to examine combining forces obtained by multiple electrodes and control of point-to-point movements. Finally, we demonstrated the feasibility of neuronal source localization using spinal surface potential recordings.

INTRODUCTION

Electrical stimulation of the nervous system is a means to restore function to individuals with neurological disorders. The objective of this project is to investigate the feasibility of neural prosthetics based on microstimulation of the spinal cord with penetrating electrodes. Specifically, chemical and viral retrograde tracers, immediate early gene expression, and immunocytochemistry are used to determine the locations and neurochemical identity of neurons in the spinal cord that control genitourinary and motor functions in the male cat. Microstimulation with penetrating activated iridium microelectrodes is used to determine the physiological effects in the genitourinary and motor systems of activation of different neural populations. Finally, inverse potential mapping is being explored as a method to determine, via spinal surface potential recordings, the location of active populations of neurons. The results of this project will provide data important to understanding neural control of genitourinary and motor functions, answer fundamental questions about microstimulation of the spinal cord, and lead to development of a new generation of neural prosthetics for individuals with neurological impairments.

PROGRESS IN THIS QUARTER

During the seventh quarter of this contract we continued a series of experiments using intraspinal injections of retrograde tracers to identify last-order interneurons that project to either the preganglionic innervation of the bladder or the pudendal motoneurons

innervating the external urethral sphincter. Secondly, we continued our experiments measuring the hindlimb motor responses evoked by intraspinal microstimulation. Finally, we continued our studies on an electrical method, using spinal surface potentials, to map the location of active neurons in the spinal cord.

Identification of Last-Order Genitourinary Interneurons

The objective of these experiments is to identify the location and rostrocaudal extent of last-order premotor interneurons that project to the pudendal motor nucleus. We used retrograde transport of fluorescent latex microspheres (Retrobeads, LumaFluor Inc., Naples, FL) and the beta subunit of cholera toxin (CTB) (List Biological Laboratories, Inc., Campbell, CA) injected into the pudendal motor nucleus to determine the distribution of last order neurons projecting to the motoneurons innervating the external urethral sphincter. Two survival experiments and one post-mortem cat experiment were conducted with post-injection survival times of 44 and 60 hours.

In the last quarter, two additional retrograde labeling experiments (B003, B004) were conducted with approximate post-injection survival times of 36 and 28 hours. The methods for animal preparation, retrograde tracer injection, animal maintenance and spinal cord harvesting and processing were essentially similar to those described in Quarterly Progress Report #7. All animal care and experimental procedures were according to NIH guidelines and were reviewed and approved by the Institutional Animal Care and Use Committee of Case Western Reserve University. Two types of retrograde tracers were used: fluorescent latex microspheres (Retrobeads, LumaFluor Inc., Naples, FL), both rhodamine and green; and the beta subunit of cholera toxin (CTB) (List Biological Laboratories, Inc., Campbell, CA).

Injection site location

We have been exploring several methods to improve localization of the targeted injection site in the rostral-caudal, dorsal-ventral and medial-lateral coordinates.

Rostral-caudal injection location

The injection site location in the rostral-caudal orientation may be located by recording cord dorsum potentials. The location of Onuf's nucleus is related to the peak evoked potentials on the surface of the spinal cord (cord dorsum potentials) resulting from stimulation of the pudendal or posterior biceps semitendinosus (PBST) nerves [Jankowska and Riddell, 1993]. The peak of the dorsum potential distributions for the posterior biceps semitendinosus (PBST) nerve (~40-50 uV) has been shown to correlate with the rostral border of Onuf's nucleus and the peak of the pudendal nerve dorsum potentials (~300 uV) has been shown to be a few mms caudal [Jankowska and Riddell,

1993]. These potentials showed no fixed relation to the L7, S1 or S2 segments, however were closely related to the levels within which Onuf's nucleus was located.

In experiment B004, dorsum potentials from stimulation of both the pudendal and posterior biceps (PB) were recorded at the ipsilateral and contralateral dorsal root entry zone. The peak dorsum potentials were located in the caudal L7 segment (~70 uV) and rostral L7 segment (~190 uV) for pudendal and PB stimulation, respectively. The rostral-caudal location of these peaks was consistent with those previously reported.

Dorsal-ventral and medial-lateral injection location orientation

Recording population potentials (field potentials) within a spinal segment may identify the injection site location in the dorsal-ventral and medial-lateral orientation. As discussed in the previous progress report, the resolution of peak field potentials within the cord based on stimulation of the whole pudendal nerve was insufficient to precisely determine the nucleus location within a penetration. Therefore injections were based on anatomical landmarks and not on direct field potential recordings.

Stimulation of the whole pudendal nerve results in both afferent and efferent evoked field potentials. Therefore in experiments B003 and B004, the urethral sphincter motor (efferent) branch was isolated and selectively stimulated instead of the whole pudendal nerve to improve the accuracy of the field potential recordings. Selective stimulation of the efferent motor branch eliminates the dorsal root afferent stimulation and should isolate the motor nucleus.

Stimulation of the urethral sphincter motor branch improved the resolution of the field potential recordings. The potentials recorded in the dorsal horn were reduced due to the elimination of afferent stimulation. However, locating the relatively small urethral sphincter motor neuron population remained challenging and we were unable to identify the center of the nucleus. Although the field potentials resulting from urethral sphincter motor branch stimulation are more specifically related to the motor nucleus, the magnitude of those potentials is reduced.

Tissue analysis

The mounting process for the fluorescent microspheres has been improved to maintain acute and long-term fluorescence. The use of xylene, which can result in tissue damage and a reduction in microsphere fluorescence, has been discontinued in the mounting process. In addition, Fluoromount mounting media should maintain long-term microsphere fluorescence and additional mounting media containing free-radical scavengers are being considered.

An additional fluorescent microscopy system (Carl Zeiss, Inc.) has been established in our laboratory. This system is connected to image processing software that

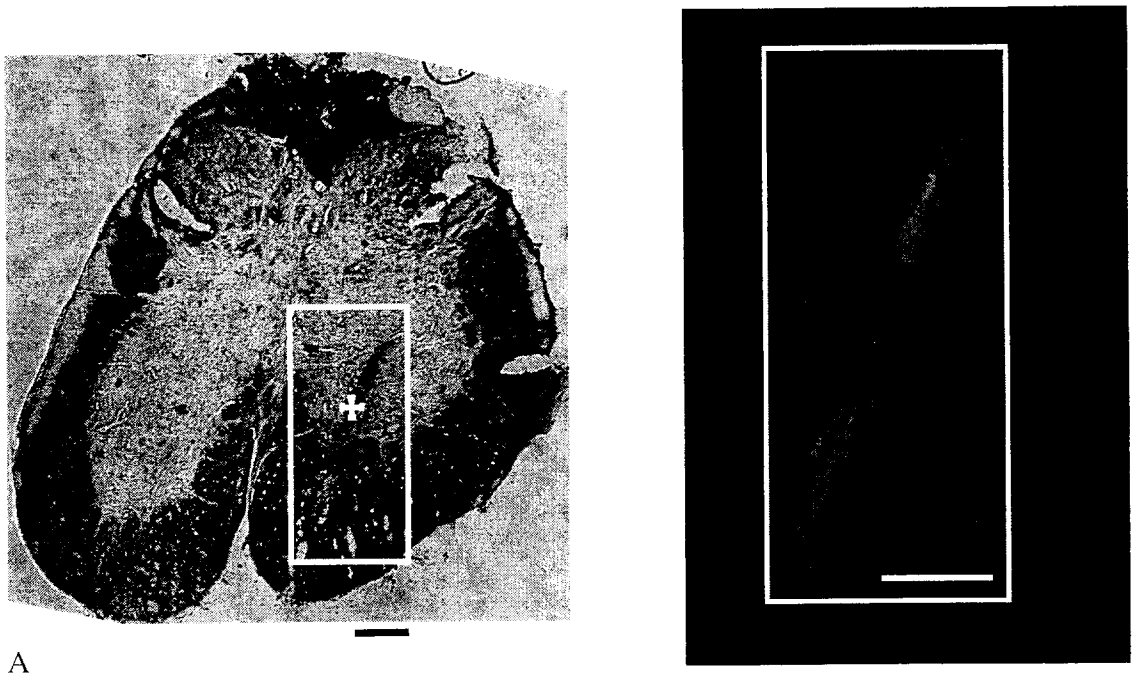

A B

Figure 1. Spinal cord cross-section from the caudal S1 segment showing the center of the rhodamine microsphere (34 nl) injection site in cat B004. A: Light micrograph. The cross hairs represent the center of the experimentally intended injection location corrected for processing shrinkage. The boxed area is expanded in B. B: Fluorescent microscope image of the injection site. Scale bars in both A and B are 500 μm.

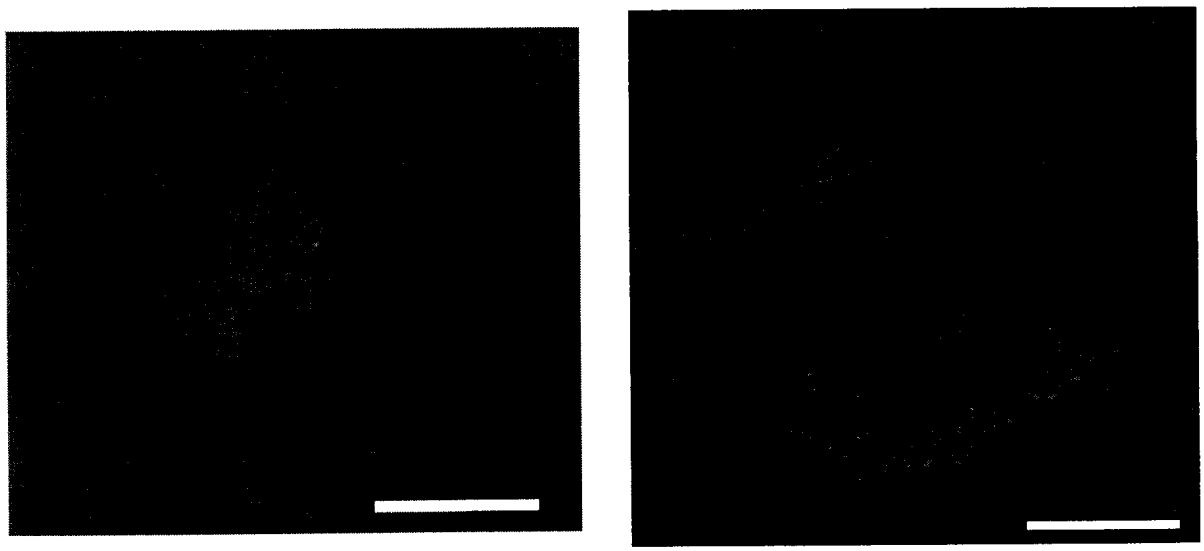

A B

Figure 2. Examples of cells retrogradely labeled with rhodamine fluorescent microspheres. A: Fluorescence microscope image of a labeled cell from the L6 segment, cat B004. Section thickness is 30 μm. Note that cell projections may be identified. B: Laser confocal microscope image of a labeled cell from the L4 segment in cat B002. Section thickness is ~ 200 nm. Scale bars in A and B are 25 and 50 μm, respectively.

allows digitized images to be obtained. This will increase availability and decrease processing time. Laser confocal microscopy resources exist and have been utilized (see figures below).

Injection site reconstruction

Histological reconstruction of the injection sites is required to validate the experimentally intended injection site location. Each injection site was identified histologically as previously described. The rhodamine microsphere injection site for cat B004 (34 nl) is shown in Figure 1. The total volume of microspheres injected was reduced from previous experiments to better match the expected size of the urethral sphincter motor nucleus.

Labeled cell identification

Retrogradely labeled cells contain fluorescent microspheres intracellularly. These cells project to neurons in the extracellular region of the injection site. Examples of retrogradely labeled cells are shown in Figure 2. Although microspheres do not label cell processes, indications of cell morphology and boundaries may be observed under fluorescent microcopy as shown in Figure 2A. The micropheres do not enter the cell nucleus, therefore the unlabeled nucleus may be identified in both Figure 1A and 1B. The laser confocal microscope allows viewing of thin sections (~100 to 200 nm) through the 30 μm histological slice. These sections may then be reconstructed into a 3-D image of the labeled cell.

Rate of retrograde transport

Experimental determination of the empirical values of retrograde transport rates in our animal model will be valuable since they determine the required post-injection times.

Retrogradely labeled neurons have been identified in the rostral end of the L3 segment, the most rostral segment harvested, for cat B002. Therefore the minimum rate of retrograde transport was ~0.8 mm/hr in experiment B002.

To date, L5 is the most rostral segment analyzed for cat B004. Retrograde labeled cells were identified in the rostral portion of this segment, therefore the minimum rate of retrograde transport was ~ 1.0 mm/hr in experiment B004. Therefore the rate is at least matches our initial conservative estimate. It is expected that retrograde transport extended rostrally and that the retrograde transport rate is greater than 1.0 mm/hr. The impact of an increased retrograde transport rate is a reduction in the post injection survival duration.

Summary of key findings

- Injection sites were identified and reconstructed in all experiments. The location and size of the injection sites were consistent with the spatial coordinates and size of the injections. Anatomical localization must still be improved.
- Retrograde labeling of spinal neurons from fluorescent microsphere injection sites was observed with both fluorescence microscopy and laser confocal microscopy.
- The minimum observed rate of retrograde transport has been increased to at least 1.0 mm/hr. Therefore total post-injection survival times may be reduced in future experiments.

Dynamic Hindlimb Motor Responses Evoked by Intraspinal Microstimulation

During the period covered by this quarterly progress report, we continued our series of measurement on force responses and motions evoked by intraspinal microstimulation of the lumber enlargement of the spinal cord. In addition, we measured the isometric force responses produced by co-activation of two spinal sites, as well as the movements generated when spinal sites were activated in succession. Surgical techniques were identical to the ones reported in earlier reports, and the robotic system described in previous reports was used to acquire the forces and motions. A brief description of the surgical methods will be given in the following paragraph, followed by a description of the robotic set-up.

METHODS

Experimental set-up

Adult cats were initially anaesthetized with ketamine (25 mg/kg), and anesthesia was maintained using gaseous halothane. A laminectomy was performed to expose the lumbar area of the cord (L4-L6), and the contralateral limb denervated. After preparation a mid-collicular decerebration was conducted and Halothane discontinued. Cord and core temperatures were maintained at 36°C, and the cord was bathed in mineral oil. Furthermore, blood pressure and expired CO_2 were monitored throughout the experiment.

The animal's pelvis was held with bone pins, and the paw was attached to a gimball mounted on a six-axis force transducer. The force transducer was mounted at the end-point of the two DOF robot described in a previous quarterly report. The robot can hold the paw isometrically during force measurements, or to be free-moving during motion measurements. The femur was not fixed and the hindlimb thus became a three link assembly, which allowed for hip motion in addition to knee and ankle motion.

Fine bifilar EMG electrodes were inserted into four hindlimb muscles (knee flexor, knee extensor, ankle flexor, and extensor) to record the electromyographic (EMG)

activity simultaneously with forces and/or motions. The raw EMG signal was amplified, filtered (10-1000Hz), and sampled at 2000Hz.

Force and Motion Measurements

Motor responses were elicited by microstimulating the cord intraspinally with trains of biphasic current pulses (train duration: 0.5 s, frequency: 40Hz, pulse duration: 100μsec, pulse amplitude: 100μA). The cord was mapped by measuring responses along dorso-ventral penetrations in increments of 200μm, at a series of positions along the rostro-caudal medial-lateral surface of the cord. At selected depths for each of the penetration the limb was moved on a 3cm grid of nine to twelve points from a mid-stance position while stimulation parameters and electrode position were kept constant. The hindlimb's end-point was moved to each of the positions on the grid by the robot, and held isometrically (stiffness: 400-450 N/m) for the duration of the trial (typically three seconds).

The forces measured at those nine to twelve locations were used to calculate the forces at the limb's end-point throughout that workspace. The workspace was divided into triangles, and the forces within a triangle were estimated by a linear interpolation based on the three vectors measured on the vertices (see Fig. 3). The forces were divided into a passive component (force measured before the onset of activation), and an active component (total forces measured minus the passive portion). Total, active and passive force fields were reconstructed.

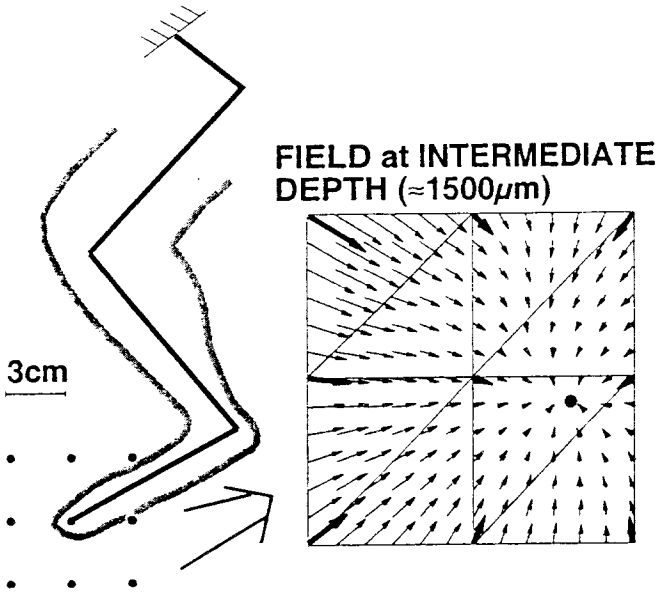

Figure 3. Force field construction. Left: spatial end-point locations where forces are recorded. The paw is moved to each of the location on the 3 cm grid with the pelvis held fixed via pins. The hip, knee and ankle are thus moved through varying range-of-motion, with the robot planar architecture preventing movements outside of the sagittal plane. Right: actual force

vectors measured (thick dark vectors), triangles dividing the workspace, and the interpolated force vectors (thin light vectors). Forces represented are the total forces (active and passive).

Hindlimb movement produced by activation of the site was also measured using the robotic apparatus. For motion measurement the robot's motors are programmed to counterbalance the weight of the linkages, thereby minimizing the apparent weight of the mechanical structure on the animal's hindleg. The action of gravity on the limb's weight is not compensated, and thus the leg starts from a fully extended position prior to stimulation onset.

Movements accomplished against programmed springs of varying stiffnesses (range 25-200 N/m) can also be measured. Springs are implemented via the robot controller with the center of the spring typically programmed to be at the mid-stance position, and the restoring force programmed to be that of a two dimensional linear stiffness spring, i.e. $F=K(X_D-X)$.

Experimental Methods for This Particular Progress Report

Two experimental designs are reported in this progress report: co-stimulation of spinal sites producing different individual responses, and movements produced by sequential activation of force fields of different structure.

a) co-stimulation of spinal sites

Two co-stimulation experiments were conducted on two animals. One electrode was inserted at the L6/L7 border ipsilateral to the limb on which forces are measured, while the other electrode was positioned on the contralateral side of the cord (both electrodes were at a depth of 800 μm, positioned 1-2 cm from each other). Activation of the ipsilateral electrode produced a flexion withdrawal response at the paw, while activation of the contralateral electrode produced a rostral extension response (limb extending forward). The individual responses for each electrode at each position were measured at one activation level. The response produced by co-activation of both sites with the stimulation levels used for the individual responses was also measured at each position. Force fields for the individual and co-stimulation responses were constructed as described above.

The relationship between individual and co-stimulation responses was tested against two hypotheses observed in previous animal preparations [Mussa-Ivaldi et al., 1994; Tresch and Bizzi, 1999]:

1) summation hypothesis: the response during co-stimulation is the scaled vector sum of the observed individual force responses, i.e. $\mathbf{F}_{AB} = s[\mathbf{F}_A + \mathbf{F}_B]$,

where $\mathbf{F}_A$, and $\mathbf{F}_B$ represent the fields obtained for stimulation at site A and B, respectively; $\mathbf{F}_{AB}$ represents the field obtained via costimulation of site A and site B. S is obtained via least-squares.

2) winner-take-all hypothesis: the response during co-stimulation is the scaled version of one of the individual responses, i.e. $\mathbf{F}_{AB} = \min\|\mathbf{F}_{AB} - s\,\mathbf{F}_{A \text{ or } B}\|$,

where $\mathbf{F}_{A \text{ or } B}$ indicates $\mathbf{F}_A$ or $\mathbf{F}_B$.

b) Movement generation via sequential activation of force fields

Movements were constructed by activating the flexor and extensor fields in sequence. This experiment was conducted with one combination of flexor and extensor fields (the two fields are the responses shown for site A & B of Fig. 4). Two sequences of activation were tested: one where the flexor field was activated first, and then the extensor field; and the second where the extensor field was activated first and then the extensor. Timing of stimulation was the same in both cases: the first field was activated at time: 1 sec for a period of 3 seconds, while the second field was activated at time: 3.5 sec for a period of 3 seconds, creating a co-stimulation interval of 0.5 second.

Movements were executed against the robot providing an upward force of approximately 3N. This force bias was obtained by programming the robot to behave as a linear spring with a stiffness of 2 N/m, and a set-point approximately 120 cm above the hip joint. The upward force bias compensated for gravity holding the limb at a mid-stance position while stimulation was off. By holding the limb at a mid-stance, we were able to better examine the leg extension created by activation of the extensor field.

RESULTS

As mentioned above, the results reported here were collected over two experiments, both using the decerebrate preparation described above.

Results for co-stimulation for the second day are shown on Figure 4. The fields obtained when each site were individually activated are shown on the top two panels, while the left bottom panel shows the force field obtained when both sites were co-activated, and the right bottom panel shows the force field obtained by summation of the two original responses. Fields' structures were compared for both angular and magnitude deviations. Sets of force vector angles, ϕ_i and φ_i, measured throughout the workspace for different sites were compared by constructing the differences $\Delta\theta_i=\phi_i - \varphi_i$, and computing the mean angle and angular deviation [Batschelet, 1981] to obtain a measure of the similarities in the angular directions of the vector measured at the same spatial location. The statistical analysis used was a Rayleigh test (at α=.01), which tests for the significance of directness, i.e. whether the data are concentrated around a point, in this

case 0°. Since the test is not very powerful we made the decision to use a 99% confidence level before rejecting the hypothesis of randomness. To compare for possible differences in the relative magnitude of fields, we measured the ratios of force vector magnitude at the sample locations in the workspace. For comparison between the actual and sum response obtained during costimulation experiments we did not normalize the vectors since in that case we were interested in comparing actual magnitudes between the costimulation response and the scaled sum of the individual responses. Ideally, this ratio should be 1.0 since force vector magnitude at the same end-point position should be the same for both fields; a *t*-test, α=.05 was used to verify the hypothesis that the ratio was 1.0. When comparing responses under the winner-take-all hypothesis, or between fields obtained at different sites, we normalized each force vector to the maximum force vector measured in the workspace for that activation.

The average orientation differences between the vectors of the fields presented in Figure 2 were not significantly concentrated around zero except for the flexor response and the actual co-stimulation response. In addition, the force magnitude ratio between the individual flexor and the scaled (s=.42±.7) co-stimulation responses was .99±.16, which is not significantly different than the desired 1.0. A similar winner-take-all behavior was observed for day one of the co-stimulation experiments.

The movements produced by sequential activation of the two individual fields depicted in Figure 3 are depicted in Figure 4. Prior to stimulation, the gravity and spring upward forces are balanced to hold the limb in a mid-stance position. Once the flexor field is activated (solid line), the limb is pulled into flexion withdrawal and remains there for approximately 2 seconds. The limb starts moving towards extension as the extensor is turned on, and extends past the initial position once the flexor field turns off. Once the extensor field activation is turned off, the limb is pulled up by the elastic forces of the spring, and would eventually settle back to its initial position (portion of the trial not collected). In the second sequence (dashed line), the limb extends rostrally when the extensor field is activated, and then moves into flexion once the flexor field is activated. Once the flexor field is turned off, the limb starts going back down. Since both fields are not convergent (as the field in Fig. 1), the movements obtained are dependent on the limb position at the onset of the field's activation. This initial position is affected by the activation sequence used, which allowed us to create two different trajectories and four holding positions with the two fields used.

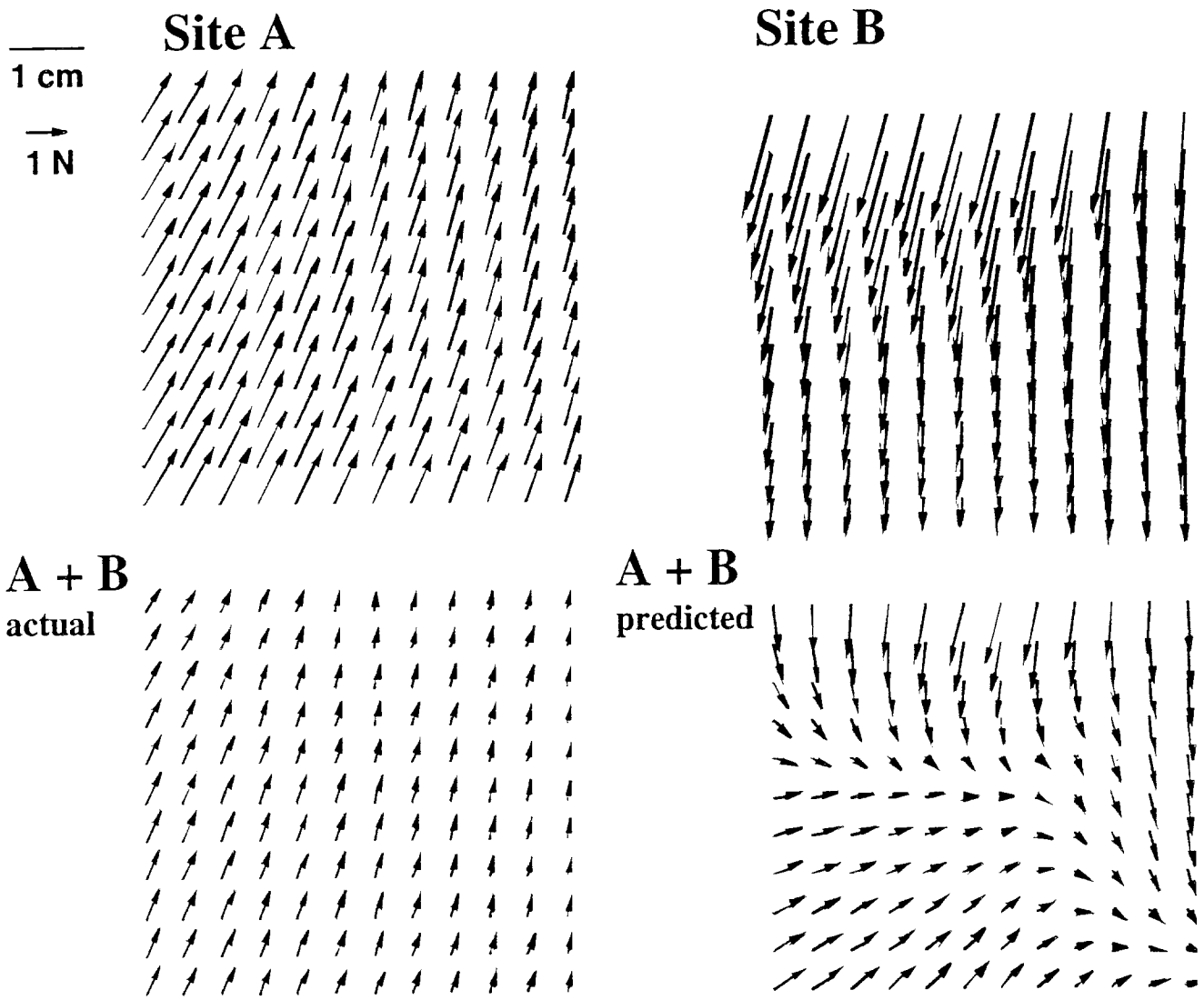

Figure 4. Force field obtained for stimulation at individual sites (two top panels), as well as the force field obtained when the two sites (A & B) are co-stimulated (bottom left panel), and the predicted summation response (bottom right panel).

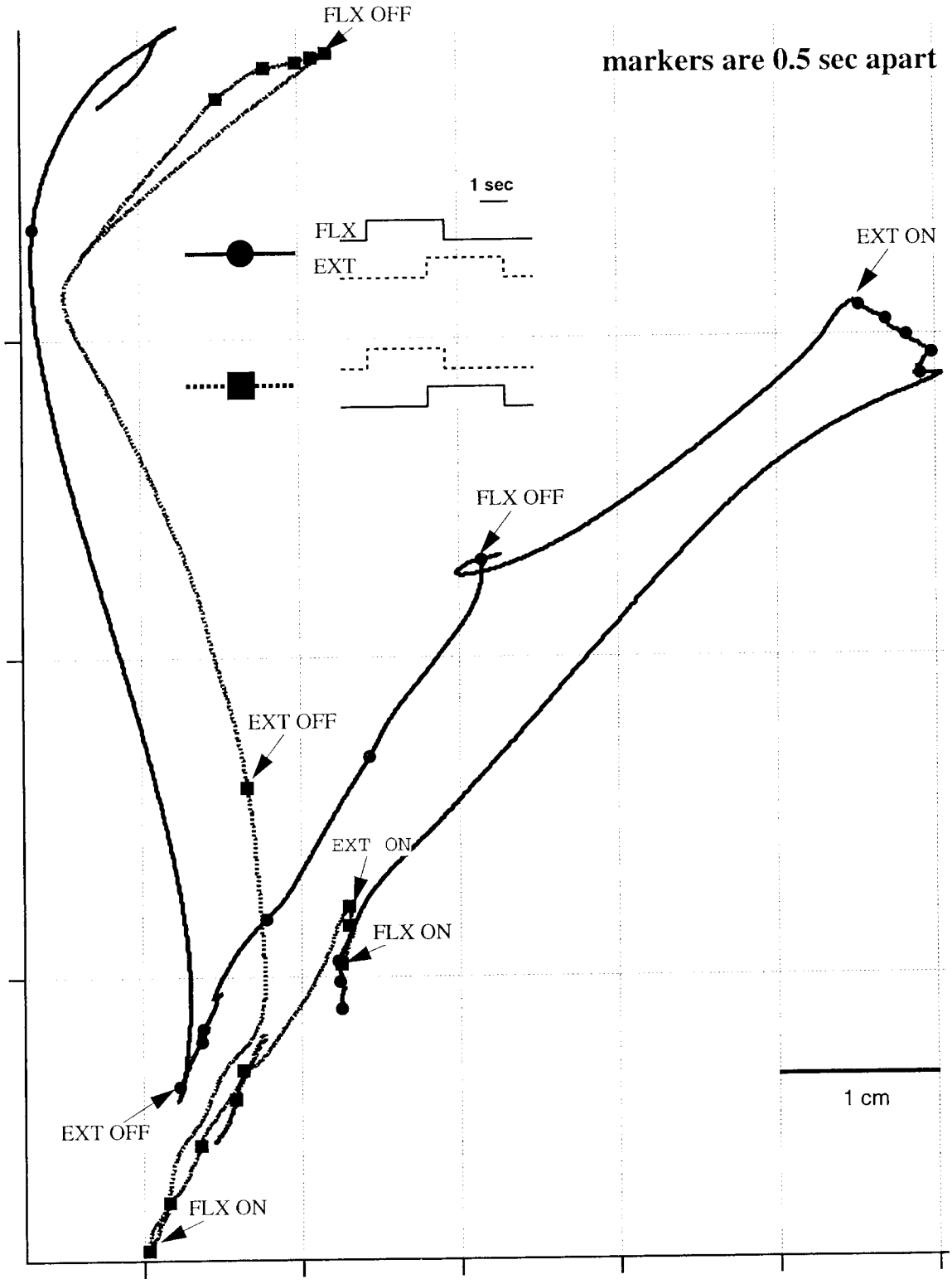

Figure 5. Trajectories created using two sequence of activation for the fields depicted in Fig. 2. The flexor withdrawal and rostral extensor fields

are sequentially activated to produced the two movements depicted. In one sequence the flexor is turned on at 1 sec for a duration of 3 sec, while the extensor field is activated at 3.5 sec for the same period of time. The order of activation is reversed in the second sequence. By alternating the activation sequence, movements with different trajectories can be created.

CONCLUSIONS

Our measurements of movements in decerebrated, spinal-intact cats indicate that the forces produced by intraspinal microstimulation are large enough to actuate the limb. The initial co-stimulation experiments reported herein show that forces during co-stimulation follow the winner-take-all behavior observed in the frog [Mussa-Ivaldi et al., 1994] and rat [Tresch and Bizzi, 1999]. The force pattern obtained during co-stimulation of spinal sites producing different responses is the scaled version of one of the individual response. Nevertheless, different trajectories can be obtained by modifying the activation sequence of the individual fields.

Development of an Intraoperative Spinal Cord Mapping Procedure

In QPR 6 we reported on the development of a volume conductor model of the spinal cord. In this quarter we have used that model to determine whether the location of intraspinal current sources (representative of active neurons) could be determined from recordings of potentials on the surface of the spinal cord. An optimization algorithm has been designed and coded in MATLAB and used in conjunction with the volume conductor model as shown in figure 6 to localize sources.

In each simulation, a point current source was randomly located within the gray matter region. The forward model was used to calculate voltages on the surface of the spinal cord model. Gaussian white noise was then added in varying amounts (variance of 0, 5, 10, or 15% of the peak surface voltage generated by the forward model). This surface potential data was then passed to the optimizer, which attempted to determine the location of the source that generated the data.

Results on the accuracy of localization are shown in figure 7. The left-hand column shows the region of the cord surface from which the optimizer was given surface potential data. The middle column shows in a cross-section of the cylinder; the dark shaded region again shows the region surface potential data that was given to the optimizer, and the light shaded region shows where the source was allowed to located for generation of the surface potential data. The latter two scenarios shown in this column reflect that experimentally we will be recording from the dorsal region of the cord to

locate sources in the ventral horn of the gray matter. The right-hand column shows the simulation results. In each case, as more noise is added, the distance between the actual source location and the optimizer-determined location increases. Furthermore, more surface potential data given to the optimizer resulted in better source localization. The results indicate that the source can be localized to within 100μm using only surface potential data from the dorsal quarter of the spinal cord, provided that the noise in less than 5%.

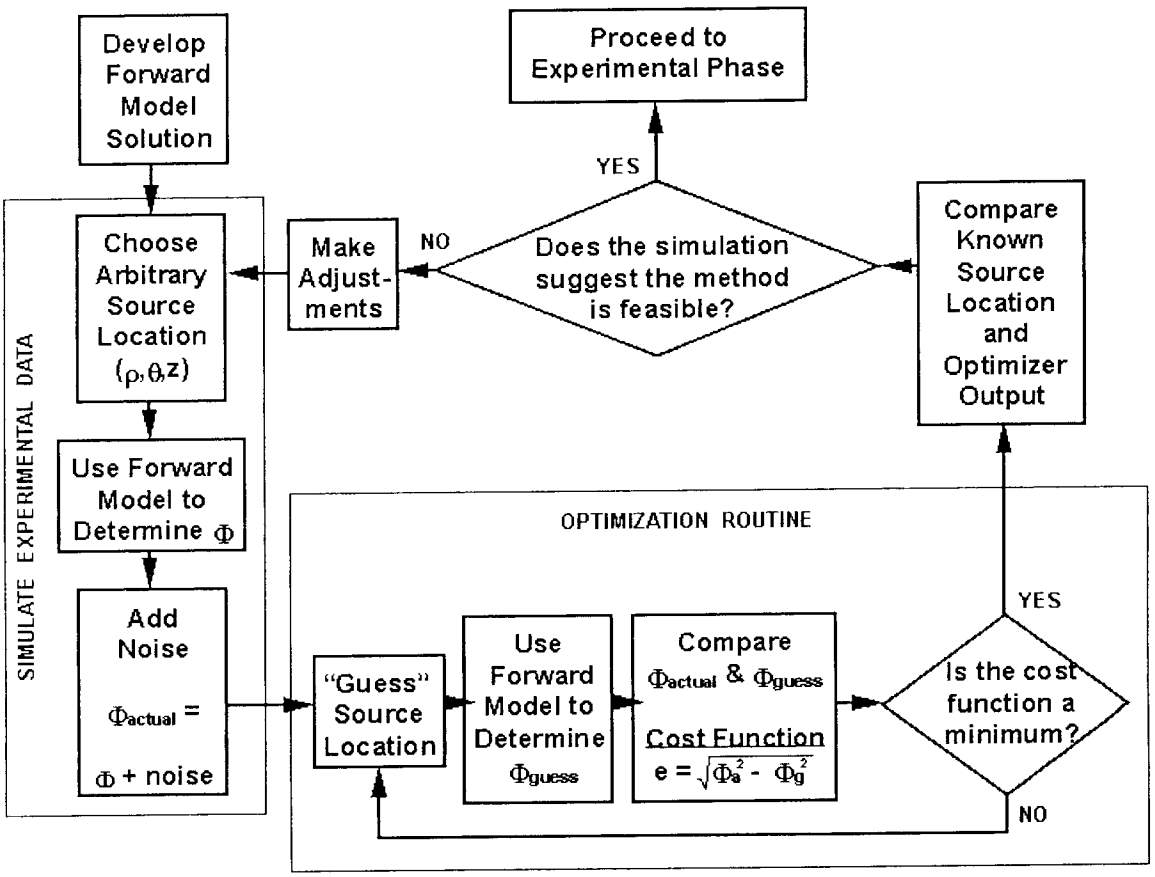

Figure 6. Block diagram of the approach to neuronal source localization using surface potential recordings.

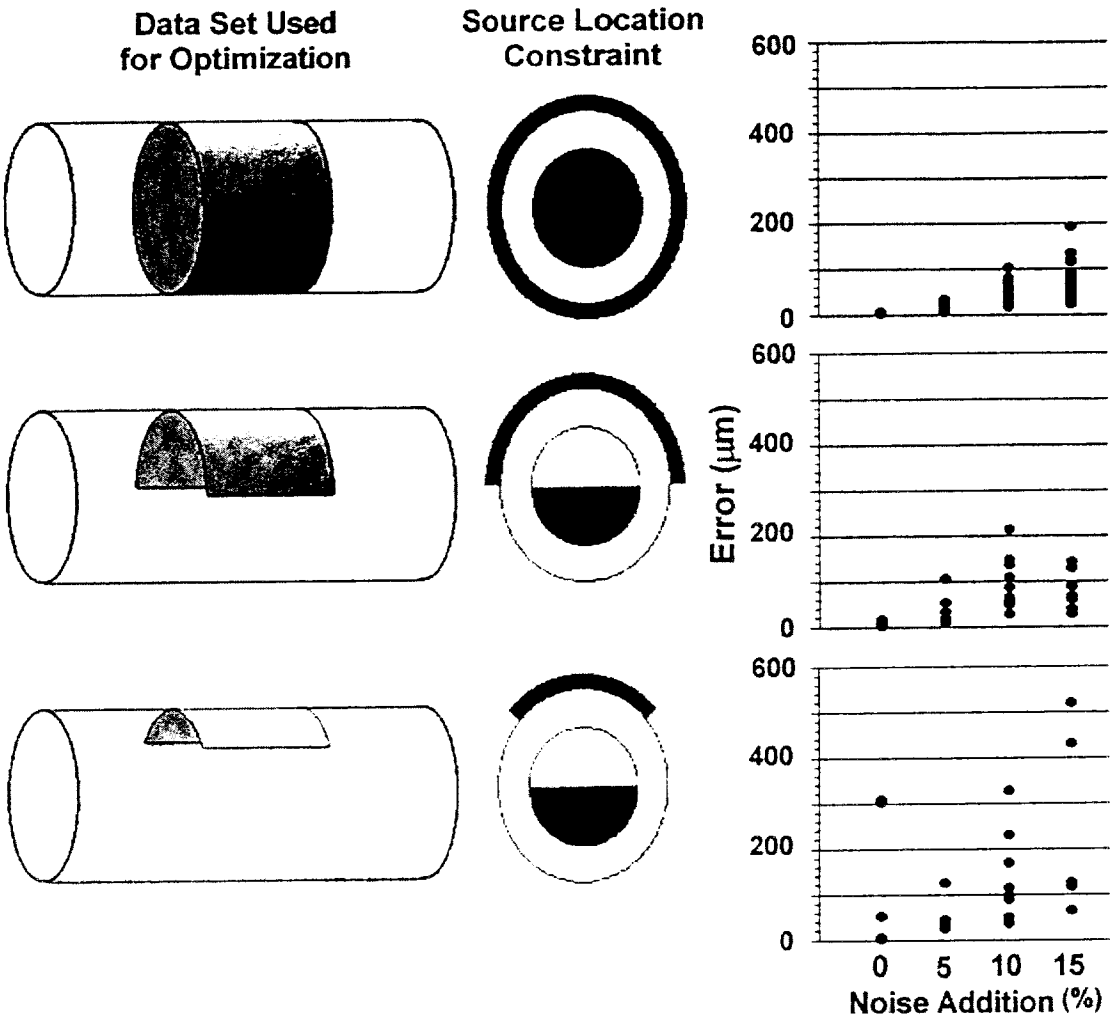

Figure 7. Accuracy of neuronal source localization using surface potential recordings for differing amounts of circumferential surface potential data and differing amounts of measurement noise.

PUBLICATIONS THIS QUARTER FROM CONTRACT SUPPORTED RESEARCH

Grill, W.M., R.F. Kirsch (2000) Neuroprosthetic applications of electrical stimulation. Assistive Technology 12(1):6-20.

Giszter, S.F., W.M. Grill, M.A. Lemay, V. Mushahwar, A. Prochazka (2001) "Intraspinal microstimulation: techniques, perspectives and prospects for FES", in: Neural prostheses for restoration of sensory and motor function, KA Moxon and JK Chapin (eds) CRC Press, pp. 101-138.

Grill, W.M., M.A. Lemay (2000) Organized hindlimb motor responses evoked by intraspinal microstimulation. Proceedings of the 5th Annual Meeting of the International Functional Electrical Stimulation Society.

Lemay, M.A., W.M. Grill (2000) Endpoint force patterns evoked by intraspinal stimulation- ipsilateral and contralateral responses in the cat. World Congress on Medical Physics and Biomedical Engineering.

Moffit, M.A., W.M. Grill (2000) Effect of source location and tissue properties on surface potentials in a cylindrical volume conductor model. Annals of Biomedical Engineering 28(Supplement 1):S112.

OBJECTIVES FOR THE NEXT QUARTER

In the next quarter we will continue our studies to identify spinal neurons which project to pudendal motoneurons. active during micturition. We will improve identification of the urethral sphincter motor-nucleus location using field potential recordings, and continue analysis of the spatial distribution of retrogradely labeled cells. We will continue our studies characterizing the hindlimb motor responses to lumbar microstimulation. Specifically, we will quantify the manner in which forces combine when sites are co-stimulated, and evaluate co-stimulation responses for sites located ipsi and contralateral to one another. We will continue our studies on electrical localization of neuronal sources. Specifically, we will continue to improve the optimization algorithm, test the efficacy of the approach when other subsets of surface potential are passed on to the optimizer, and characterizing the ability of the optimizer to localize the source as a function of source location.

LITERATURE CITED

E. Batschelet, Circular Statistics in Biology. New York: Academic Press, 1981.

Hoover, J.E., R.G. Durkovic (1992) Retrograde labeling of lumbosacral interneurons following injections of red and green fluorescent microspheres into hindlimb motor nuclei of the cat. Somatosens. Motor Res. 9:211-226.

Jankowska, E., J. S. Riddell (1993). A relay for input from group II muscle afferents in sacral segments of the cat spinal cord. J Physiol (Lond) 465:561-80.

F. A. Mussa-Ivaldi, S. F. Giszter, and E. Bizzi, "Linear combinations of primitives in vertebrate motor control," *Proc. Natl. Acad. Sci. USA*, vol. 91, pp. 7534-7538, 1994.

Nadelhaft, I, W.C. DeGroat, C. Morgan (1980) Location and morphology of parasympathetic preganglionic neurons in the sacral spinal cord of the cat revealed by retrograde axonal transport of HRP. J. Comp. Neurol. 193:265-286.

Shefchyk, S. J., R. R. Buss (1998). Urethral pudendal afferent-evoked bladder and sphincter reflexes in decerebrate and acute spinal cats. Neurosci Lett 244(3):137-140.

Thor, K.B., C. Morgan, I. Nadelhaft, M. Houston, W.C. de Groat (1989) Organization of afferent and efferent pathways in the pudendal nerve of the female cat. J. Comp. Neurol. 288:263-279.

M. C. Tresch and E. Bizzi, "Responses to spinal microstimulation in the chronically spinalized rat and their relationship to spinal systems activated by low threshold cutaneous stimulation," *Exp. Brain Res.*, vol. 129, pp. 401-16, 1999

Ueyama, T. N. Mizuno, S. Nomura, A. Konishi, K. Itoh, H. Arakawa (1984) Central distribution of afferent and efferent components of the pudendal nerve in cat. J. Comp. Neurol. 222:38-46.

Van Buren, J.M., K. Frank (1965) Correlation between the morphology and potential field of a spinal motor nucleus in the cat. Electroenceph. Clin. Neurophys. 19:112-126.

Vanderhorst, V.G.J.M., and Holstege (1997) Organization of lumbosacral motoneuronal cell groups innervating hindlimb, pelvic floor, and axial muscles in the cat. J. Comp. Neurol. 382:46-76.